In vivo imaging of alphaherpesvirus infection reveals synchronized activity dependent on axonal sorting of viral proteins

Andrea E. Granstedt[a,b], Jens B. Bosse[a,b], Stephan Y. Thiberge[b,c], and Lynn W. Enquist[a,b,1]

[a]Department of Molecular Biology, [b]Princeton Neuroscience Institute, and [c]Lewis-Sigler Institute for Integrative Genomics, Princeton University, Princeton, NJ 08544

Edited by Elliott Kieff, Harvard Medical School and Brigham and Women's Hospital, Boston, MA, and approved August 2, 2013 (received for review June 22, 2013)

A clinical hallmark of human alphaherpesvirus infections is peripheral pain or itching. Pseudorabies virus (PRV), a broad host range alphaherpesvirus, causes violent pruritus in many different animals, but the mechanism is unknown. Previous in vitro studies have shown that infected, cultured peripheral nervous system (PNS) neurons exhibited aberrant electrical activity after PRV infection due to the action of viral membrane fusion proteins, yet it is unclear if such activity occurs in infected PNS ganglia in living animals and if it correlates with disease symptoms. Using two-photon microscopy, we imaged autonomic ganglia in living mice infected with PRV strains expressing GCaMP3, a genetically encoded calcium indicator, and used the changes in calcium flux to monitor the activity of many neurons simultaneously with single-cell resolution. Infection with virulent PRV caused these PNS neurons to fire synchronously and cyclically in highly correlated patterns among infected neurons. This activity persisted even when we severed the presynaptic axons, showing that infection-induced firing is independent of input from presynaptic brainstem neurons. This activity was not observed after infections with an attenuated PRV recombinant used for circuit tracing or with PRV mutants lacking either viral glycoprotein B, required for membrane fusion, or viral membrane protein Us9, required for sorting virions and viral glycoproteins into axons. We propose that the viral fusion proteins produced by virulent PRV infection induce electrical coupling in unmyelinated axons in vivo. This action would then give rise to the synchronous and cyclical activity in the ganglia and contribute to the characteristic peripheral neuropathy.

Alphaherpesviruses are pathogens of the mammalian nervous system that often evoke manifestations of peripheral pain or itching after infection. The severity and extent of symptoms vary depending on the herpesvirus strain and the host. Herpes simplex virus (HSV) and varicella-zoster virus (VZV) infections in humans characteristically cause lesions that are preceded by sensations of localized pain, which also sometimes lasts long after lesions have been cleared (1, 2). Pseudorabies virus (PRV) is a swine alphaherpesvirus that is related to HSV and VZV. Whereas in its natural porcine host PRV establishes latency in the peripheral sensory ganglia, in nonnative animal hosts, including laboratory mice, PRV causes a severe acute peripheral neuropathy called the "mad itch" (3). This neuropathy is characterized by a strong impulse to bite and scratch the skin of the infected dermatome feverishly and incessantly, which results in severe self-inflicted wounds (4). PRV has proved useful for elucidating pathways involved in the manifestation of these clinical symptoms. Specific PRV gene products have been identified as virulence factors and these research efforts have led to successful live vaccines, such as the strain PRV Bartha and its derivatives (see ref. 5 for review). Despite this effort, the molecular basis for the pronounced peripheral neuropathies produced by PRV and the other alpha herpesviruses remain an active area of research.

In the 1950s, Dempsher and colleagues recorded spontaneous bursts of neuronal activity in rat sympathetic superior cervical ganglia (SCG) infected with virulent PRV and the onset correlated with the mad itch symptomology (6). Other in vivo studies showed that the activity induced by PRV infection was reversibly blocked by curare and was cholinergic in origin (7, 8). Denervation of the preganglionic nerve before infection did not affect mad itch symptoms, yet no spontaneous electrical discharges were recorded in the ganglia (8). These studies suggested that increased infection-induced electrical activity originated in the presynaptic terminals within the ganglia (8, 9). A recent publication examined the electrical activity of homogenous cultures of peripheral nervous system (PNS) neurons from the SCG infected with virulent or attenuated PRV strains in vitro using patch clamp recordings (10). They found that neurons infected with a virulent PRV strain had increased and sustained rates of action potential firing late in infection that were synchronized among the neuronal population. Infection by the attenuated PRV strain Bartha exhibited a marked delay in the onset of abnormal firing. Importantly, these studies showed that the PRV membrane fusion protein glycoprotein B (gB) was required for elevated firing rates and fusion of infected neuron cell bodies. The authors concluded that fusion pores were formed during PRV infection, which enabled ions to flow between neurons to cause direct electrical coupling (10). As the pores increased in size, spontaneous action potentials spread into coupled neurons and throughout the network, causing firing events to synchronize

Significance

Pseudorabies virus (PRV), an alphaherpesvirus related to human herpes simplex and varicella-zoster viruses, causes the characteristic "mad itch" in which infected animals scratch an afflicted area until self-mutilation. The mechanism by which PRV induces these symptoms is still poorly understood, and most work has been done in limited systems in vitro. Here we report studies performed in living mice. We observed that infection with a virulent PRV strain induces synchronous and cyclical neural activity, but this activity disappears during infection with a vaccine strain that does not cause mad itch. We demonstrate the aberrant activity depends on a viral fusion protein, and its trafficking specifically into axons. These findings correlate the disrupted physiology to the known neuropathy in vivo.

Author contributions: A.E.G. and L.W.E. designed research; A.E.G., J.B.B., and S.Y.T. performed research; A.E.G. and J.B.B. contributed new reagents/analytic tools; A.E.G., J.B.B., and S.Y.T. analyzed data; and A.E.G., J.B.B., S.Y.T., and L.W.E. wrote the paper.

The authors declare no conflict of interest.

This article is a PNAS Direct Submission.

[1]To whom correspondence should be addressed. E-mail: lenquist@princeton.edu.

This article contains supporting information online at www.pnas.org/lookup/suppl/doi:10.1073/pnas.1311062110/-/DCSupplemental.

and resonate in the culture. This synchronous firing phenomenon also manifests itself as a continuous and rapid calcium flux in infected cultured neurons that can lead to other dramatic changes, including changes in mitochondrial shape and dynamics (11). Therefore, the formations of viral-induced excitatory synaptic connections that allow for continuous propagation of action potentials do not reflect normal chemical transmission at conventional synapses, but rather an abnormal coupling that requires viral DNA replication and that can be strain dependent (12, 13).

Whereas the results with cultured neurons suggested a mechanism by which PRV may induce neuropathy, the relatively simplified in vitro system still leaves unanswered questions about what happens during infection of animals. In particular, studies using the mouse flank scarification model showed that virulent and attenuated PRV strains, such as PRV Bartha, have two different mechanisms of neuroinvasion and lethality in mice (4). Specifically, the virulent strain induces the classic symptomology of violent pruritus with rapid onset of death, little viral antigen in the brain, and no signs of CNS pathology. In contrast, mice infected with PRV Bartha survive much longer, do not exhibit any peripheral neuropathy, have abundant infectious virus in the brain, but do present CNS abnormalities at very late times after infection and still succumb (4). Therefore, it appears that during infection with virulent PRV strains, but not attenuated PRV Bartha strains, the infected peripheral neural circuits are the primary players in determining the severe clinical manifestations. Our previous study in living mice showed that a PRV Bartha recombinant, expressing a genetically encoded calcium indicator, did not induce synchronous activity among neurons in an autonomic ganglia (14), However, we did not examine neuronal activity after virulent PRV infection. The differences between in vitro and in vivo infections are obvious, such as the organization of innervated tissues, structure of ganglia, and the involvement of glial cells, but their impact on infection and symptomology after infection with virulent or attenuated PRV strains is not clear.

In this report, we examined neuronal activity during a virulent PRV infection of anesthetized mice by imaging infected PNS ganglia directly in vivo. To do so, we constructed virulent and mutant PRV recombinants that expressed the genetically encoded fluorescent calcium indicator protein GCaMP3 (15). This calcium sensor fluoresces in the presence of calcium transients and is therefore a useful correlate of neuronal activity (16). Calcium imaging enabled us to monitor the activity in vivo of multiple infected neurons simultaneously with single-cell resolution using two-photon microscopy. Interestingly, 2 d after infection of the salivary glands by virulent PRV, infected neurons in the submandibular ganglia (SMG) flashed synchronously and cyclically. There were no qualitative signs of fusion between soma in the ganglia. When we severed the axons between the brainstem and the ganglia in vivo and continued imaging, the flashing phenotype continued unabated, suggesting that the impetus to fire did not arise in the presynaptic brainstem neurons. In contrast, infection by a replicating, but attenuated PRV-Bartha–derived recombinant that does not cause violent pruritus showed no signs of synchronous or cyclical firing even at later times after infection. In addition, mutants that do not express either viral gB involved in membrane fusion or viral membrane protein Us9 required for sorting and transport of virions and viral glycoproteins such as gB in axons, showed no signs of synchronous or cyclical firing. These data validate in vivo the in vitro observation that virulent PRV infection induces electrical coupling via fusion events. Importantly, we further propose that in vivo, this electrical coupling may occur in the infected, unmyelinated axons that bundle together as they project to the salivary gland, and therefore the spatial organization of natural synaptic partners in vivo would contribute to the specific phenotype, which cannot be distinguished in vitro. Our in vivo evidence supports the hypothesis that the peripheral neuropathy observed during a virulent PRV infection in living mice results from sustained, aberrant firing of infected PNS neurons.

Results

Virulent PRV Infection Causes Synchronous and Cyclical Calcium Transients Among Neurons. We inserted the calcium sensor G-CaMP3 into the glycoprotein G (gG) locus of the viral genome of the virulent wild-type strain PRV Becker by homologous recombination (PRV 468; *Materials and Methods* and Fig. S1). Viral protein gG is not essential for spread in vivo (17), and many of the commonly used PRV circuit tracing strains contain insertions at this locus (18). We infected the salivary glands of adult mice with PRV 468 and monitored the spontaneous calcium activity in the peripheral submandibular ganglia of anesthetized mice using two-photon microscopy (schematic in Fig. 1*A*). We used the changes in fluorescence as a correlate of neural activity. The calcium traces are normalized to the background fluorescence and therefore displayed as the relative change in fluorescence ($\Delta F/F$). The preparation for in vivo imaging was as described previously (14) and allowed us to image the calcium flux of many infected neurons in a field of view simultaneously with single-cell resolution. We chose 40–48 h postinfection (h.p.i.) as our imaging window because at this time point, disease symptoms produced by a virulent infection are not pronounced, yet essentially every neuron in the SMG is infected, as indicated by the fluorescent signal from GCaMP3 (picture in Fig. 1*B*).

By imaging a population of individually infected neurons, we observed that neurons in the ganglia were flashing synchronously and cyclically (Fig. 1*B* and Movie S1). All participating cells initiated each new calcium peak concurrently. We quantified the correlation of calcium flux between neurons using Pearson's coefficients of correlation. In this analysis, the pairwise coefficients between all neurons in a ganglion were computed, and the correlation increases as the coefficients approach 1. The distribution clearly indicated a strong positive correlation (Fig. 1*C*): when one cell experienced an increase in calcium flux, there is a high likelihood that another cell would also experience an increase in calcium flux. As a result, neurons of the infected ganglia appear to be flashing synchronously. The synchronous calcium transients also presented in a quasicyclical pattern, which persisted for the duration of each imaging session without interruption. The pattern was produced at fairly regular intervals, despite noise and occasional short delays in frequency. We analyzed the distribution of interpeak intervals in a histogram with 1-s bins (Fig. 1*D*). In this example, the prominent peak occurred at 10 and 11 s, demonstrating the overall regularity of the calcium pulses. These synchronous and cyclical calcium patterns strongly suggested a mechanism of electrical coupling to account for the synchronous and cyclical activity between neurons.

The spiking phenotype was reproducible across many infected mice. We analyzed the interpeak intervals of calcium transients from five different infected animals. The calcium events occurred every 5–15 s or in frequency range between 0.1 and 0.2 Hz, with occasional differences (Fig. S2). In one animal, we were able to acquire data from two different ganglia. The flashing signals in each ganglion were similar, but each maintained a unique interpeak interval distribution, suggesting that the ganglia are independent from each other and not interconnected even though they all innervate the same infected salivary gland (Fig. S2).

The data shown in Fig. 1 *B–D* were taken at a time resolution of approximately two frames per second. By using faster rates of image acquisition, we determined the extent to which cells fired synchronously. We imaged at the fastest possible rate of our system using a line scan to achieve a time resolution of 758 sampling points per second. At this time resolution, some slight delays between traces were detected that ranged between 50 and 100 ms (Fig. S3). The histogram in Fig. S3 presents the results of the differences in peak timing for the two cell bodies in which

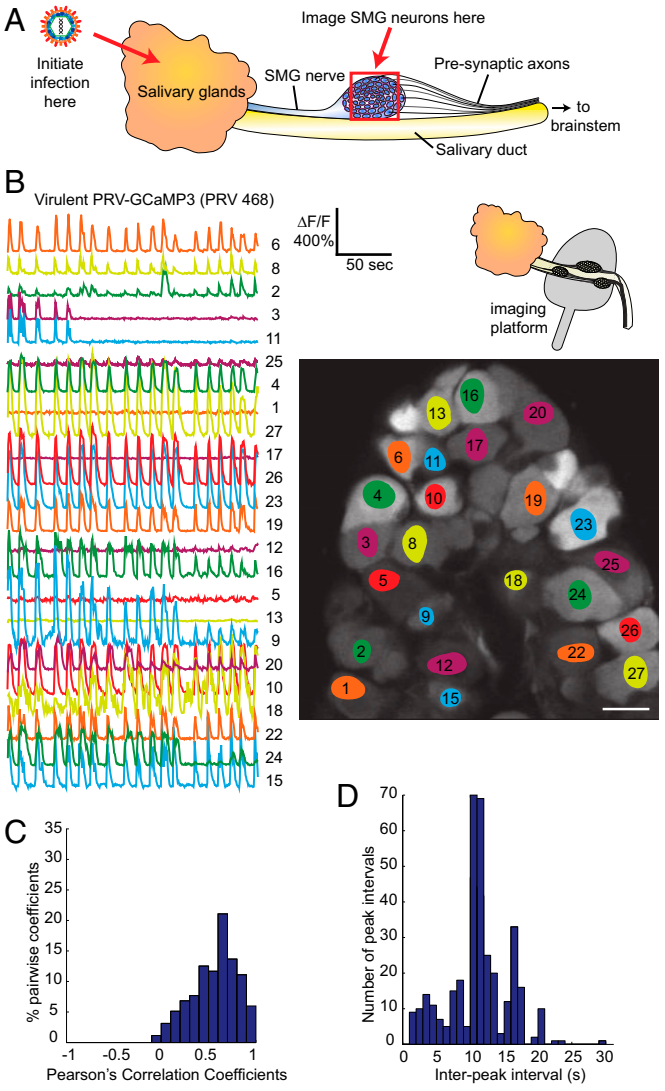

Fig. 1. Neurons infected with PRV 468 display a synchronous flashing phenotype. (*A*) Simplified schematic of in vivo infection and imaging locations (red arrows and red box) within the salivary circuit. Key components of salivary circuit are outlined, not to scale. The salivary glands are inoculated with PRV and 2 d later, the submandibular ganglia (SMG) are imaged in living mice. (*B*) Calcium traces from neurons infected with virulent PRV 468 expressing GCaMP3. Schematic shows the setup for in vivo imaging in which the SMG ganglia are lifted on an imaging platform. Picture displays a representative field of view in which a population of individually infected neurons in the SMG was imaged simultaneously. The superimposed colored areas highlight the regions of interest within each cell from which the corresponding normalized ΔF/F calcium traces (numbered) were computed. The relative fluorescence change (ΔF/F) and timescale are indicated. (Scale bar, 50 μm.) (*C*) Quantification of the correlation of calcium flux between neurons using a histogram of Pearson's coefficients of correlation. Pairwise coefficients between neurons in a ganglion were computed and coefficients binned in 0.1 increments to generate a distribution. All features of the calcium traces, such as amplitude, shape, and noise, were included in the analysis between each pair. The histogram indicates a strong correlation. (*D*) Distribution of interpeak intervals in a histogram with 1-s bins.

a segment of their measured traces are displayed. Twenty-nine successive peaks are included in this distribution, which shows a mean difference of 68 ms. These slight delays suggest that if electrical coupling is occurring in the salivary circuit, the coupling likely exists at some distance from the neuron cell bodies that were imaged.

Each Cell Has a Unique Calcium Peak Shape. We noticed that although neurons presented synchronous and cyclical calcium transients, the calcium traces of individual cells were not identical in amplitude and duration. In fact, for the duration of the observations, each synchronously flashing cell appeared to exhibit a unique calcium peak shape profile. We analyzed this phenomenon at faster frame rates for data acquisition using the line scan parameters noted above. Fig. 2 shows four different cells in which the calcium peaks of each cell were superimposed. Each cell displayed a calcium peak of unique shape, amplitude, and duration that are remarkably consistent. For example, cell 1 displays very weak fluorescence changes that are slightly above the background noise. Cell 2 exhibits calcium flashes that average 150% above background at their peak, and these calcium levels plateau for a full second before beginning to decrease and return to background. Cell 3 also peaks around 150% above background, but the calcium levels immediately begin to decrease after peaking. Cell 4 displays much higher changes in calcium flux, averaging close to 500% above background. The unique calcium traces of individual neurons suggest that electrical coupling of cell bodies in the ganglion is unlikely, and therefore coupling could be taking place in distant axons.

The Spiking Phenotype Does Not Require Connections from CNS Neurons That Project to the SMG. As previously mentioned, the close synchrony of calcium flux between SMG neurons was reminiscent of electrical coupling as reported in published work in vitro (10, 11) and therefore suggested that a similar mechanism could be occurring somewhere within the salivary circuit, although to date viral-induced fusion pores have not been demonstrated in vivo. If electrical coupling were to occur in the salivary circuit, we reasoned that possible sites would include the neurons of the superior salivatory nucleus (SSN) in the brainstem that are presynaptic to the SMG, the cell bodies of neurons in the SMG, or in the SMG axons that project to the salivary glands.

The SMG ganglia receive input from the SSN, which lies in the lateral reticular formation of the pons in the brainstem. The preganglionic axons branch to innervate one of more neurons in the SMG, but each neuron in the SMG receives input from only one cell in the SSN (19). These brainstem neurons are in close proximity to one another and not ensheathed by glial cells and therefore could possibly become electrically coupled by viral-induced fusion events causing synchronous firing in each SMG. We tested this possibility by severing SSN axonal inputs to the SMG (schematic in Fig. 3*A* shows the location of axon cuts). We first prepared infected animals for imaging as before and imaged the synchronous and cyclical calcium activity for several minutes (Fig. 3*B* and Movie S2). We then clamped and held the preganglionic bundle of axons and surrounding tissue with a hemostat and cut the axons and tissue below. We immediately resumed imaging and observed that the synchronous and cyclical flashing continued unabated (Fig. 3*C* and Movie S3). We quantified the correlation of calcium flux between neurons and the distributions clearly indicated a strong positive correlation (Fig. 3 *D* and *E*). These experiments demonstrate that brainstem nuclei are not essential to elicit the spiking phenotype.

Our data also suggest coupling is unlikely to occur among infected SMG cell bodies for several reasons. We observed cyclical and synchronous flashing in cells that were not adjacent and we never observed any overt fusion or syncytial events between SMG cell bodies. Furthermore, there were slight delays between the onset of the calcium peaks across cells and individual infected neurons had unique calcium peak profiles. Finally, because each SMG neuron is ensheathed by one or more satellite cells, the SMG cell bodies are physically insulated from any fusion events. The next possibility is that coupling occurs in SMG axons that project to the salivary gland, which we further explored using attenuated and mutant PRV recombinants.

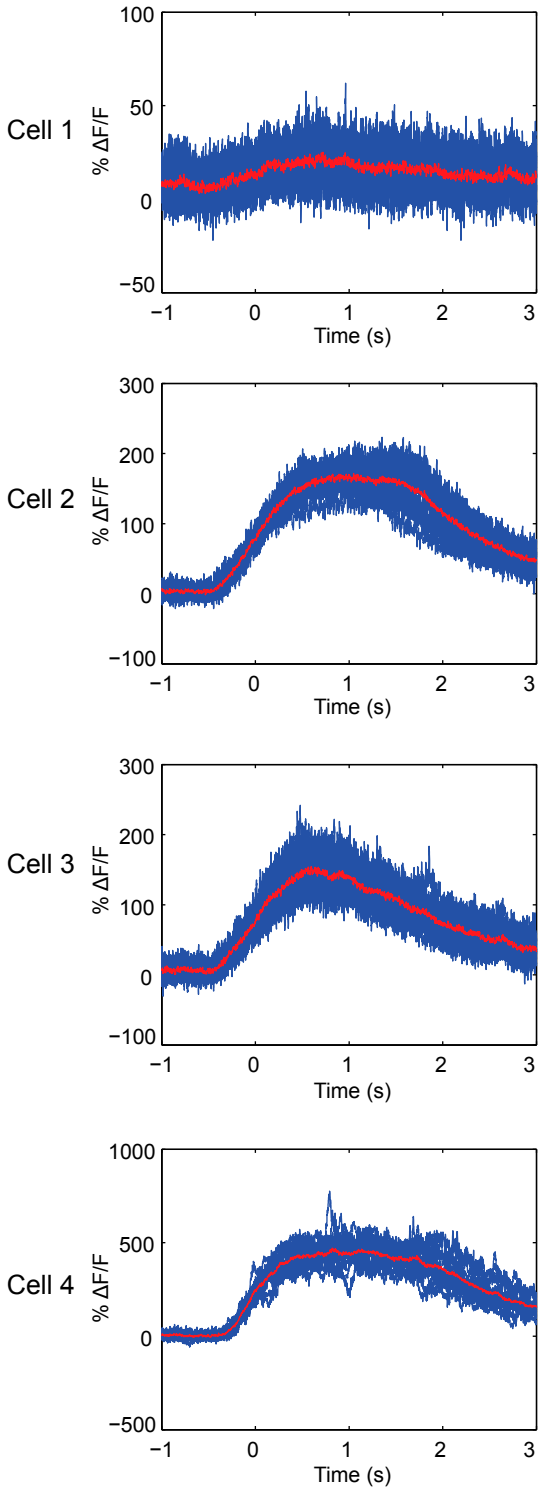

Fig. 2. Each infected cell has a unique calcium peak profile. Superimposed calcium traces from four individual cells are displayed. All four cells are from the same line scan measurement. The peaks were overlaid by aligning the inflection points in the rising portion of the peaks. Averaged peak profiles are shown in red. Data show a superimposition of at least 16 peaks for each cell.

Spontaneous Calcium Spiking Is Not Observed During Infection with an Attenuated Strain. PRV Bartha is an attenuated live vaccine strain that replicates well, yet exhibits markedly reduced pathogenesis with no mad itch symptomology. PRV Bartha harbors many mutations in its genome; in particular, it contains a deletion that includes the glycoproteins E and I, and the viral membrane protein Us9 (20, 21). These three viral gene products are required for sorting viral proteins and virions into axons (22). As a result, PRV Bartha and its derivatives are widely used in tracing neuronal circuitry because infection spreads unidirectionally from postsynaptic neurons to presynaptic neurons (Fig. 4*A*).

We constructed a PRV strain isogenic with PRV Bartha with the GCaMP3 cassette inserted in the gG gene (PRV 469; *Materials and Methods* and Fig. S1). We infected animals with PRV 469 and monitored spontaneous calcium activity at 72 h after infection. Most of the SMG neurons were infected and exhibited complex but asynchronous calcium events that were unique to each cell as we had reported previously using a less sensitive sensor (GCaMP2) (14). The changes in fluorescence (ΔF/F) in neurons infected with PRV 469 were bright and often exceeded 200% (Fig. 4*B* and Movie S4). Importantly, even at 72 h after infection, we never observed any synchronous or cyclical calcium spiking activity among neurons. There was no indication of any correlation (Fig. 4*C*) and no evidence of cyclical spiking (Fig. 4*D*). These data suggest that the axonal sorting of viral proteins and anterograde transport of infectious virus in the SMG axon bundles projecting back to the salivary glands are crucial to the development of the synchronous flashing phenotype observed during a virulent PRV infection.

The Spiking Phenotype Requires Viral Fusion Protein gB and Viral Sorting Protein Us9. The experiments with PRV 469 indicated that viral proteins were required in SMG axons that project to the salivary gland to produce the spiking phenotype. Previous published work showed that electrical coupling in cultured infected neurons was due to fusion events promoted by the viral fusion protein gB, because gB null mutants did not promote microfusion events between neuronal soma in vitro (10). The virion fusion protein gB is essential for infection by virus particles where it promotes fusion of the viral envelope with the cell. In addition, gB is required for spread of infection to secondary neurons or neighboring cells (23). Therefore, we constructed a PRV mutant that was isogenic with the virulent PRV 468 strain, but lacked the gene for viral fusion protein gB (PRV 935; *Materials and Methods* and Fig. S4). We propagated PRV 935 on complementing gB producing cells so that the virus stock produced could infect once upon initial inoculation to the salivary glands, either by infecting the salivary gland cells or by infecting directly the axon terminals projecting from the SMG neurons. After PRV 935 infection of the salivary gland, we observed a small number of infected neurons in the SMG (Fig. 5*A*). Because complemented gB null virions can infect only once, these neurons must have been infected directly at axon terminals in the salivary gland. However, among those infected neurons, none showed a synchronous calcium flux (Fig. 5*A* and Movie S5). In addition, the transients were not correlated (Fig. 5*B*). These results suggest that fusion and spread promoted by gB are important to the spontaneous generation of synchronous calcium activity among infected neurons in the SMG. It is important to note that PRV 935 cannot spread any further than the SMG because replication in those neurons produces viral progeny with no gB. We propose that the synchronous and cyclical flashing of GCaMP3 is caused by electrical coupling of infected SMG axons that project to the salivary gland and that this coupling results from gB-driven axonal fusion events.

A caveat to this interpretation is that very few SMG neurons were infected by the gB null mutant. Accordingly, we constructed a PRV mutant that was isogenic with the virulent PRV 468 strain, but lacked the viral membrane protein Us9 gene (PRV 936; *Materials and Methods* and Fig. S4). Us9 is necessary for sorting and transport of viral structural proteins, including gB, and virions into axons (24). Without Us9, PRV spreads unidirectionally in the retrograde direction both in vitro and in vivo (25, 26). The attenuated PRV Bartha strain lacks the Us9 gene,

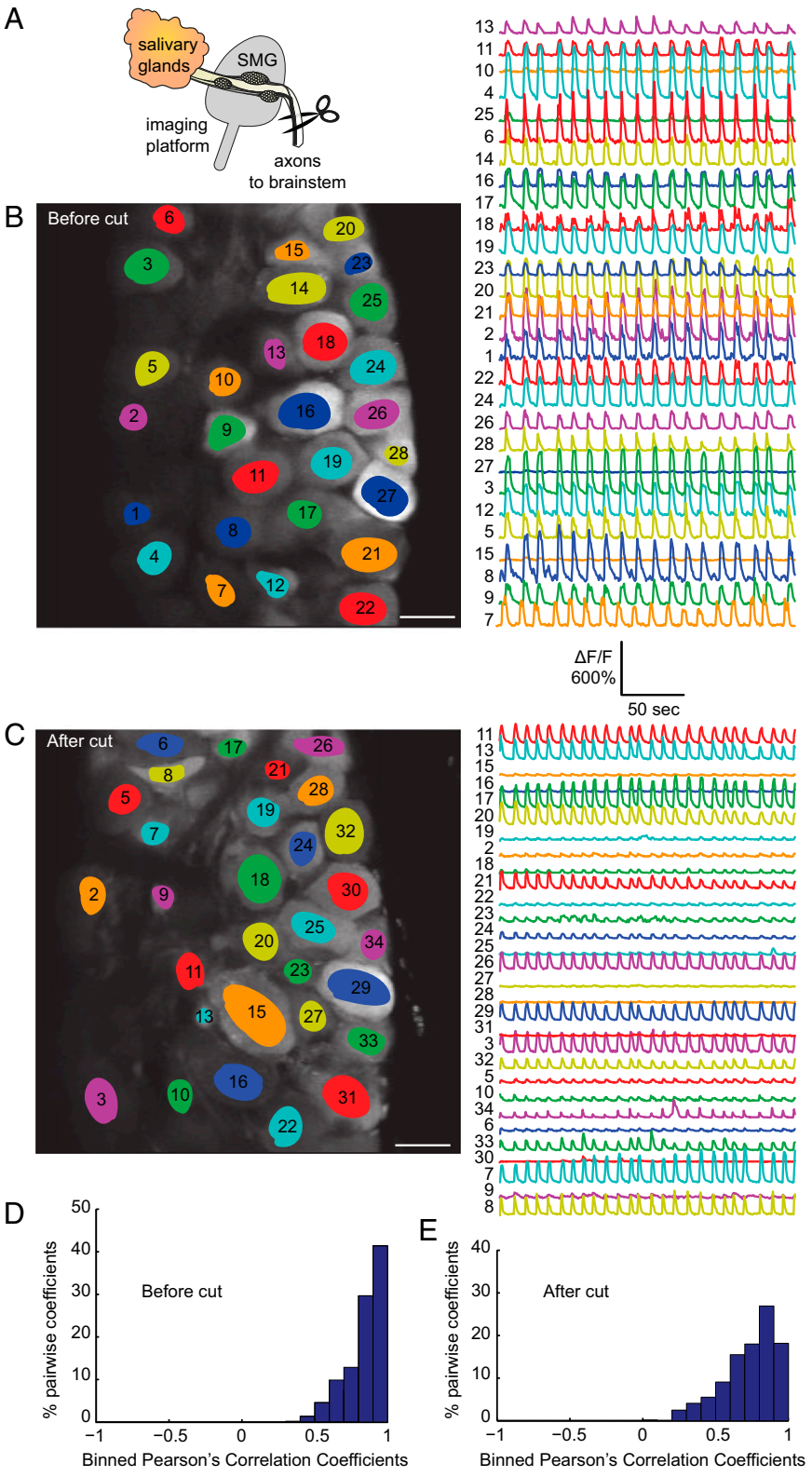

Fig. 3. The flashing phenotype persists despite severing brainstem connections. (*A*) Schematic indicating the location of the axonal cuts. We used a hemostat to clamp and hold the preganglionic bundle of axons from the brainstem and surrounding tissue and then cut everything below. We always verified that all tissue had been cut afterward by removing the hemostat and ensuring that nothing remained below. Spontaneous activity was first imaged for several minutes before cutting (*B*) and then immediately after cutting (*C*). Pictures display the fields of view in SMG with individually highlighted neurons. The corresponding calcium traces are the relative fluorescent changes normalized to the background fluorescence (ΔF/F). (Scale bar, 50 μm.) (*D* and *E*) Histograms of Pearson's coefficients indicate a strong correlation before and after the cut.

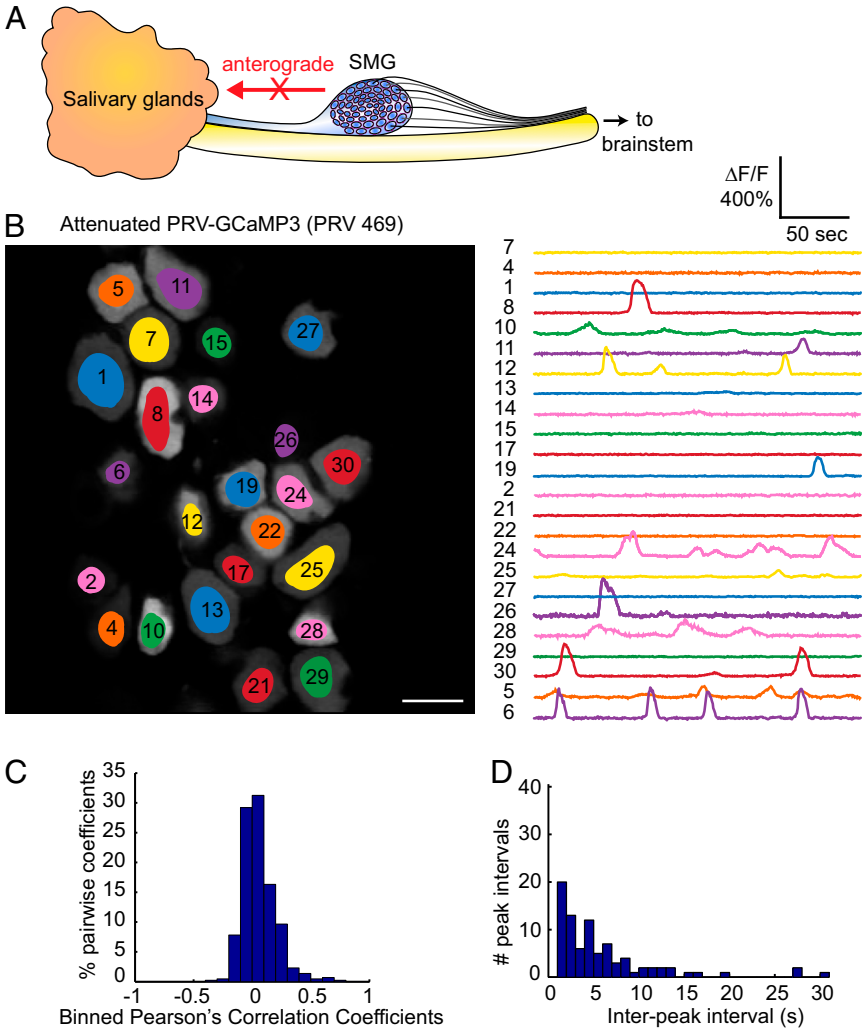

Fig. 4. Infection with the attenuated PRV 469 does not elicit synchronous flashing. (*A*) Schematic highlighting the retrograde limited phenotype of PRV 469. (*B*) Field of view of an SMG infected with PRV 469, with highlighted regions of interest in each neuron and corresponding spontaneous calcium traces. (Scale bar, 50 μm.) (*C*) The absence of correlation between cells is reflected in the histogram of Pearson's coefficients being centered on zero. (*D*) Histogram of interpeak intervals did not reveal any significant peak above noise.

which accounts in large part for its retrograde-only spread phenotype (21). HSV and VZV both have Us9 homologs with similar subcellular localization and membrane topology (27). We infected the salivary glands of mice with PRV 936 and imaged the SMG in vivo 2 d later. By this time postinfection, the majority of cells in the SMG were infected. Importantly, no synchronous or cyclical spiking activity was detected (Fig. 5*C* and Movie S6). Neurons flashed independently without any correlation (Fig. 5*D*). These results strongly suggest that anterograde transport and spread of virions and virion proteins in axons are essential for the production of synchronous calcium flux among infected SMG neurons. Taken together, the PRV 935 and 936 infection data indicate that newly made viral proteins produced in primary infected SMG neurons are sorted in a Us9-dependent process into the unmyelinated axons that project back to the salivary gland. These newly produced viral proteins could induce electrical coupling in closely apposed axons, most likely by gB-mediated fusion events, leading to abnormal SMG firing patterns.

Discussion

In this report, we imaged in vivo the activity of PRV-infected neurons by fluorescent protein expression of the genetically encoded calcium indicator, GCaMP3. We inoculated the salivary glands of mice with various PRV recombinants expressing GCaMP3 and observed that after infection by virulent PRV, peripheral neurons in the SMG exhibited highly correlated synchronized and cyclical GCaMP3 transients, reminiscent of viral-induced electrical coupling events published in vitro (10, 11). Interestingly, whereas remarkably synchronous, the calcium peak shapes were distinctive in amplitude and duration from neuron to neuron. We detected 50- to 100-ms delays in the calcium transients between pairs of neurons, but only at the highest data acquisition rate. The calcium transients were cyclical with a frequency range between 0.1 and 0.2 Hz, with slight variation among ganglia. These results suggested the possibility of electrical coupling in the infected salivary gland circuit distant from the SMG cell bodies. Changes in intracellular calcium levels also have been reported after PRV infection of cultured PNS neurons (11). In that study, synchronous calcium transients were detected by labeling neurons with a calcium sensitive fluorescent dye. The onset of these events coincided with the timing of increased firing rates in vitro, and were proposed to result from electrical coupling (11).

In contrast to virulent PRV infection, infection with the attenuated PRV-Bartha–derived recombinant expressing GCaMP3

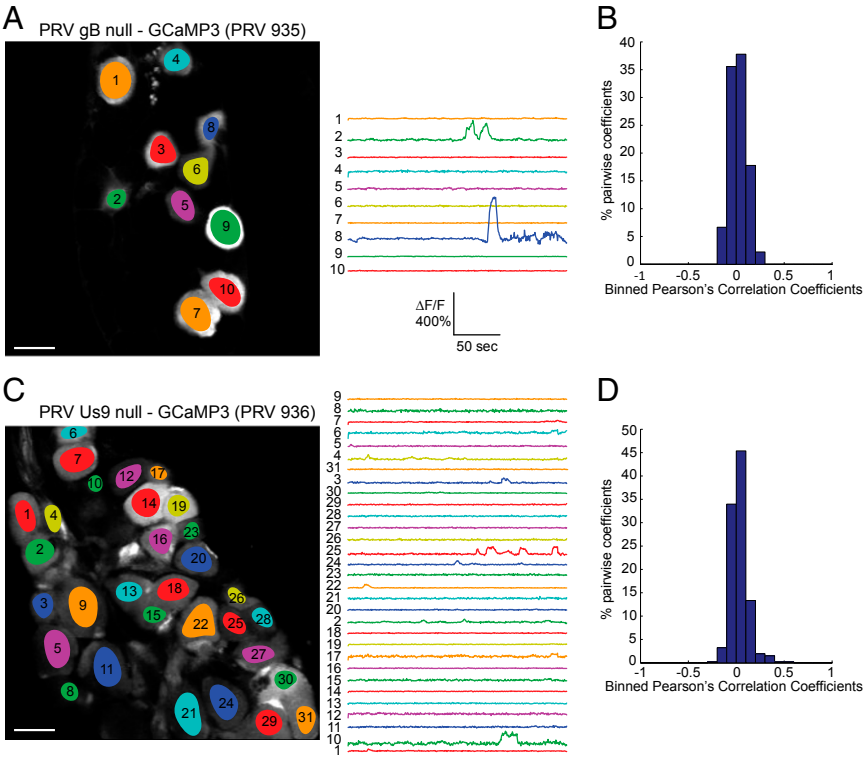

Fig. 5. Infection with either a gB null strain or a Us9 null strain does not elicit synchronous flashing. (*A*) Few neurons are infected after inoculation with the gB null strain PRV 935, but no spontaneous synchronous activity is detected among these cells. (Scale bar, 50 μm.) (*B*) Histogram of Pearson's coefficients indicated no correlation between cells infected with PRV 935. (*C*) The majority of cells are infected after inoculation of the Us9 null strain PRV 936, yet the spontaneous calcium signals are not synchronous. (Scale bar, 50 μm.) (*D*) Histogram of Pearson's coefficients indicated no correlation between cells infected with PRV 936.

showed no signs of synchronous or cyclical firing despite efficient infection of the ganglia. Rather, the neurons exhibited random calcium transients with no correlation between neurons. These results are consistent with our previous published work using a PRV Bartha recombinant expressing the less sensitive indicator GCaMP2 (14). Other in vivo transsynaptic analysis using PRV Bartha derivatives as circuit tracers also have reported no dramatic alteration in the physiological properties of infected neurons (17).

Our data showed that the CNS projections to the SMG were not involved, that each neuron cell body displayed a unique calcium peak profile, and that the attenuated PRV-Bartha–derived recombinant, which spreads only from postsynaptic to presynaptic neurons, did not display the synchronous and cyclical flashing phenotype. These data suggested that electrical coupling was occurring at some distance from the ganglia, most likely in the axons that project from the SMG to the salivary glands. To test this hypothesis, we imaged the SMG after infection with PRV mutants lacking either the viral glycoprotein B, involved in membrane fusion, or the viral membrane protein Us9, required for sorting and transport of virions in axons. We focused on these two viral proteins based on previous work; other viral proteins are also involved in membrane fusion, such as the gH/gL complex, or anterograde spread, such as the glycoprotein E (gE)/glycoprotein I (gI) complex, but we did not explore their potential role in the firing phenotype in these experiments. Neither the gB or Us9 null mutant PRV infections showed any signs of synchronous or cyclical firing. Because Us9 is essential for sorting gB into axons (24), and the attenuated PRV-Bartha–derived recombinant expresses gB but not Us9, we propose that the transport of newly made virions and virion proteins into SMG axons that project back to the gland may be essential for the generation of synchronous and cyclical calcium flux. The synchronous and cyclic firing in the ganglia would occur by virally induced fusion in the infected, unmyelinated bundled axons that project to the salivary glands.

The concept of a functional interaction between closely apposed infected axons has been noted before for PRV. Using modified Campenot chambers and cultured SCG neurons, Ch'ng and colleagues showed that PRV infection could spread between neurons at sites of axoaxonal contact (28). Furthermore, in various in vitro models, virions can egress at axonal varicosities (23, 29). Other axon–axon interactions in the absence of infection have been described in the hippocampus for ultrafast neuronal communication (30). One computational analysis of this CNS phenomenon revealed that electrical coupling between axons induces synchronous oscillations with cell body action potentials evoked antidromically from the axon (31). In the PNS, ultrastructural studies have demonstrated sites of axoaxonal synapses between sympathetic and parasympathetic nerves innervating the same peripheral target (32), and these sites of contact have functional significance (33). Sensory and autonomic postganglionic axons are usually unmyelinated, and groups of axons are surrounded by Schwann cells in troughs termed "Remak bundles" (34, 35). These unmyelinated sites could facilitate infection-induced axoaxonal coupling in the salivary circuit.

The model developed and characterized here was the salivary circuit, where infection is initiated at the salivary glands, and the peripheral parasympathetic SMG are imaged. The glands also receive motor sympathetic efferent input from the superior cervical ganglia, as well as somatic sensory afferent innervations from the trigeminal ganglia (36). The afferent supply is considered to be of the same origin as the trigeminal sensory innervations of the oral and nasal mucosa, and therefore this model is

also relevant to disease models of HSV-1, which naturally infects the trigeminal ganglia.

A further important aspect of in vivo PRV infection in the SMG model is the concept of "round-trip" reseeding and amplification of infection in the ganglia. By imaging acute explants of the SMG and surrounding tissues after in vivo PRV infection of the salivary glands, we have recently reported that newly made particles in infected SMG neurons are transported back to the glands where the infection was initiated (37). These particles then infect more axons in the gland and return to infect additional neurons in the ganglia, which in turn leads to more infection in the gland. This reseeding phenomenon occurs only with a virulent virus infection and not with PRV Bartha or Us9 null infections (37). It is likely that reseeding of the infected gland contributes to massive invasion of the innervating PNS ganglia and involvement of more axons in electrical coupling. We suggest that this round-trip infection process contributes significantly to the characteristic peripheral neuropathy of PRV infection.

Our current observations may explain the known symptomology of PRV infection, particularly the characteristic neuropathy of the mad itch. We suggest that the major cause is infection-induced, synchronous, and cyclical firing in PNS ganglia that project to the infected tissues, which results from fusion pore formation in unmyelinated axons of infected neurons. In this model, a normal action potential is "short circuited" by leaking ions into fusion-coupled axons, which in turn leads to back-propagated signals that induce more firing. These sites of gB-mediated microfusion and current leakage may occur at varicosities or other places of functional interaction among axons. Fusion events could occur between PNS ganglia cell bodies as shown with cultured SCG neurons in vitro (10). However, in the SMG, and in other PNS ganglia, cell bodies are sheathed by satellite glial cells that restrict direct contact of neurons and probably inhibit viral spread between neuronal cell bodies (34).

Importantly, we found that infection by the PRV Bartha recombinant, which does not induce any peripheral neuropathy, also does not induce synchronized or cyclical firing in neurons. We suggest that PRV Bartha cannot induce electrical coupling in the unmyelinated SMG axons because it lacks the Us9 protein required for sorting virion proteins into axons. We have been able to propose a model that accounts for the differences between the virulent and attenuated strains because we used an in vivo system in which the spatial organization of tissues and synaptic partners are preserved.

There is circumstantial evidence in the literature to suggest that virulent alphaherpesviruses may spread laterally in peripheral sensory ganglia (see ref. 38 for review). In the mouse flank model, herpes simplex virus and PRV inoculations at a single site result in spread throughout the innervated dermatome, suggesting disseminated spread in the sensory dorsal root ganglia (DRG) (4, 39). Fusion of neurons and satellite cells has been demonstrated in human DRG xenografts in mice infected with varicella-zoster virus (40). In addition, virulent PRV infection of the mouse flank results in substantial viral titers recoverable in visceral organs, but not in an infection with attenuated PRV Bartha (4); infection of sensory neurons that project to internal organs could be accounted for by lateral spread in the DRG because these visceral afferent neurons reside concomitantly in sensory ganglia (38). Our model could account for these observations.

The violent pruritus induced by virulent PRV infection has several components. First, the animal appears to perceive a consistent and continuous irritation that stimulates itching motor activity. The animal is then consumed by this behavior, without stopping to eat, drink, or groom (4). By observing the calcium profiles of many SMG neurons simultaneously with single-cell resolution, we characterized synchronous and cyclical patterns of activity that were highly correlated among infected neurons. This phenotype is reminiscent of the spontaneous bursting activity in infected sympathetic ganglia associated with behavioral pruritus (6). Our studies suggest that common mechanisms may exist that induce alterations in PNS physiology leading to severe neuropathic pain caused by human alphaherpesvirus infections (e.g., disseminated herpes zoster or postherpetic neuralgia).

Materials and Methods

Cells and Virus Construction. PRV 468 and PRV 469 were constructed by homologous recombination between a plasmid containing a GCaMP3 expression cassette and the gG locus of the PRV Becker and PRV Bartha genomes, respectively. The plasmid pN1-GCaMP3 was a gift of Charles Zuker (Columbia University, New York, NY) and contains the coding sequence of GCaMP3 in place of EGFP in the pEGFP-N1 plasmid, under the control of a cytomegalovirus immediate-early (CMVIE) promoter (Clontech; GenBank accession no. U55762). The pN1-GaMP3 plasmid was linearized and cotransfected into swine epithelial (PK15) cells with DNA from PRV 616, a PRV Becker derivative, or PRV 614, a PRV Bartha derivative, and both these parental strains have mRFP1 inserted into the gG locus (18). Homologous recombination of the GCaMP3 cassette into the gG locus of PRV 616 or PRV 614 was directed between the CMVIE promoter and the simian virus 40 (SV40) polyadenylation sequences, replacing the original 2.3-kb mRFP cassette at this locus with the 2.5-kb GCaMP3 cassette. Resulting recombinants were plaque purified on PK15 cells by selection of nonred plaques. The recombinants were crossed with a PRV Becker or PRV Bartha derivative that expressed an mRFP capsid fusion protein (PRV 180 and PRV 765, respectively). Double recombinants were plaque purified three times so that the final strains PRV 468 and PRV 469 expressed diffusible GCaMP3 as well as a red capsid tag. These recombinants enabled us to independently confirm infection of cells and expression of GCaMP3. Restriction fragment length polymorphism (RFLP) analysis using SalI was used to compare PRV Becker, PRV Bartha, PRV 468, and PRV 469, confirming the correct integration of the GCaMP3 cassette (Fig. S1*A*). Nucleocapsid DNA was prepared using standard protocols (41). To check for robust protein expression of the inserted cassette, we performed a Western blot using the following antibodies: polyclonal rabbit anti-GFP (Invitrogen; A11122), mouse anti major capsid protein VP5 (42), and the monoclonal mouse anti–beta-actin (Sigma; A1978) (Fig. S1*B*). For the single-step growth curve, PK15 cells were infected at a multiplicity of infection of 10, with input virus removed by saline washes after 1 h. Each time point was performed in triplicate and titered in duplicate (Fig. S1*C*).

PRV 935 was constructed by homologous recombination between pHF22 (43), which has a gB deletion and NsiI/PvuI linearized pII-GCaMP3, a derivate of pII (17) in gB-complementing cells. pII-GCaMP3 was made by exchanging the EGFP coding DNA sequences (CDS) of pII with the GCaMP3 CDS of plasmid GCaMP3, provided by Loren Looger (Janelia Farm Research Campus, Ashburn, VA) (15) through Addgene (Addgene; plasmid 22692). Briefly, a 1370-bp fragment of the plasmid GCamp3 ranging from its BglII to the NotI site (position 628–1998) coding for the complete GCaMP3 CDS was recombined with pII at its EcoRI and NotI sites (position 1544–2316) by the proprietary cloneEZ technology (Genscript).

PRV 936 was constructed by homologous recombination similar to the construction of PRV 935. Nucleocapsid DNA of PRV 325 (26, 44) that carries a mRFP-VP26 fusion and a Us9 deletion was recombined with HindIII linearized pUC-gG-GCaMP3 as described above. pUC-gG-GCaMP3 is similar to pII but is smaller and genetically more stable. It is based on pUC57-gG-multiple cloning site (MCS), which was made by inserting a synthetic construct between the NdeI and HindIII sites of pUC57 (Genscript). The inserted synthetic construct consists of 850 bp of homology to the surroundings of the PstI site in the US4 locus of PRV Becker, into which a pCMV-IE-MCS-SV40 polyadenylation sequences cassette was inserted. The GCaMP3 CDS of GCaMP3 (Addgene; plasmid 22692) was then subcloned into the MCS of pUC57-gG-MS between the BglII/NotI sites (Genscript).

PRV 935 was characterized by Western blotting using the monoclonal antibody M2 against gB (45) (Fig. S4*A*). For the characterization of PRV 936 we used polyclonal rabbit antisera directed against Us9, gE, and gI (46–48) to probe for the expression of Us9, gE, and gI, respectively (Fig. S4*B*).

Infection of Mouse SMG. All animal procedures were performed in accordance with the guidelines of the National Institutes of Health and were approved by local authorities (Princeton University Institutional Animal Care and Use Committee). This preparation for mouse SMG infection was previously published (49). Briefly, adult male mice aged roughly 7–10 wk were anesthetized with a mixture of ketamine (100 mg/kg) and xylazine (10 mg/kg) by i.p. administration. A midline incision was made along the neck, exposing the salivary glands. Using a Hamilton syringe, an aliquot of concentrated

PRV inoculum (1×10^9 pfu/mL) was injected into both submandibular glands (5 μL/side). The incision was sutured and the mice were given buprenorphrine (100 μg/kg concentration) for postsurgical pain. The mice were allowed to recover for various times after infection.

In Vivo Calcium Imaging. The protocol for imaging infected SMG in living mice was repeated from our previous publication (14), and more details are provided in the published protocol (49). Briefly, mice were anesthetized in an isofluorane chamber and then transferred in supine position to a custom-built stage with heating pad, rectal temperature probe, and nose cone for isoflurane inhalation. A ventral midline incision was made along the neck and the skin was pulled back with retractors. The SMG were exposed and lifted on a small custom-made metallic platform, controlled by a micromanipulator. The area was perfused with warmed artificial cerebral spinal fluid containing (in millimoles): 127 NaCl, 25 $NaHCO_3$, 1.25 NaH_2PO_4, 2.5 KCl, 1 $MgCl_2$, and 25 glucose. The animal's temperature was maintained at 35 °C.

Live imaging was performed using a custom-built two-photon scanning microscope (50) built around an upright Olympus BX51. Fluorescence photons were collected through a 40×, 0.8 N.A. Olympus water immersion objective LUMPlanFl/IR, and detected with high quantum efficiency GaAsP photomultiplier tubes (H10770PA-40; Hamamatsu). The microscope was operated by the Matlab software ScanImage (51). Images were taken with an excitation wavelength of 920 nm provided by a tunable Ti:Sapphire laser (Chameleon; Coherent Inc.). Movies were recorded at various scan rates.

Image Analysis. The two-photon raw data were analyzed directly in Matlab using custom-written code. To correct for the lateral movements induced by the animal, the images were first aligned and registered automatically. Then the software drew regions of interest (ROI) around each infected cell and these ROI were subsequently confirmed manually. ROI for cells bodies missed by the software were added manually. The mean pixel intensity F(t) in each ROI was then extracted for every time point to obtain a time-series fluorescence trace for each ROI (ΔF/F). Slow timescale changes in the fluorescence traces (e.g., due to photobleaching or small drift in the z focal position) were removed by determining the distribution of fluorescence values in a 20-s interval around each sample time point and subtracting the eighth percentile value. The value of 20 s was chosen because it is much longer than the duration of a calcium transient observed. The eighth percentile value was found to be appropriate to isolate the baseline F_0. The normalized baseline-subtracted fluorescence traces $[(F(t) - F_0)/F_0$, noted in text as ΔF/F] for each ROI were then further analyzed to measure the correlation between the fluorescent signals of different neurons. Correlations were computed from Pearson's coefficients of correlation. The pairwise correlation coefficients of a given ganglion were displayed in histograms of 0.1-width bins. Interpeak interval analysis on low time resolution data only (movies taken at 2 ms per line, 256 × 256, 256 × 128, and 256 × 64 pixels) was performed using a threshold method. ΔF/F traces were smoothed using a high-frequency filter and times at which ΔF/F reached the threshold value were measured. Subtractions of successive time values gave the interpeak intervals. The results for each cell were displayed in histograms of 1-s bins. We performed high time resolution experiments by scanning single lines (line scans at t = 1 and 2 ms) crossing usually three or four cell bodies. Regular images of the whole field of view were recorded before and after the experiment to check for possible drift along the optical axis. The data were discarded in the rare cases this drift was significant. The segments of the line associated with each cell body were then treated as ROIs and processed in Matlab, as described above. The peak timing analysis relying on arbitrary threshold values was not appropriate for measuring the calcium transient delays between cells. To address the timing of an individual cell's calcium transients, a method independent of the actual ΔF/F values was necessary, and the onset of the signal or the inflection point was measured. We chose to quantify the timing of the calcium transient by measuring the time values when the second derivative of ΔF/F cancels (while going from positive to negative value, i.e., in the rising portion of the fluorescence signal). These time values were then used to measure interpeak intervals and cell-to-cell delays and to realign all peaks from a given cell body.

ACKNOWLEDGMENTS. We thank the members of the L.W.E. laboratory for their input and discussions, and particularly M. L. Szpara and O. Koyuncu for their detailed feedback on the manuscript. This research was funded by National Institutes of Health (NIH) Grants NS033506 and NS060699. The Imaging Core Facility at the Lewis-Sigler Institute is funded by NIH National Institute of General Medical Sciences Center Grant PM50 GM071508.

1. Cohen JI, Straus SE, Arvin AM (2007) Varicella-zoster virus replication, pathogenesis, and management. *Fields Virology*, eds Knipe DM, Howley PM (Lippincott Williams & Wilkins, Philadelphia), 5th Ed, Vol 2, pp 2773–2818.
2. Pellett PE, Roizman B (2007) The family *Herpesviridae*: A brief introduction. *Fields Virology*, eds Knipe DM, Howley PM (Lippincott Williams & Wilkins, Philadelphia), 5th Ed, Vol 2, pp 2479–2499.
3. Mettenleiter TC, Ehlers B, Muller T, Yoon K-J, Teifke JP (2012) Herpesviruses. *Diseases of Swine*, eds Zimmerman JJ, Karriker LA, Ramirez A, Schwartz KJ, Stevenson GW (Wiley, New York), 10th Ed, pp 421–446.
4. Brittle EE, Reynolds AE, Enquist LW (2004) Two modes of pseudorabies virus neuroinvasion and lethality in mice. *J Virol* 78(23):12951–12963.
5. Mettenleiter TC (2000) Aujeszky's disease (pseudorabies) virus: The virus and molecular pathogenesis—state of the art, June 1999. *Vet Res* 31(1):99–115.
6. Dempsher J, Larrabee MG, Bang FB, Bodian D (1955) Physiological changes in sympathetic ganglia infected with pseudorabies virus. *Am J Physiol* 182(1):203–216.
7. Dolivo M, Honegger P, George C, Kiraly M, Bommeli W (1979) Enzymatic activity, ultrastructure and function in ganglia infected with a neurotropic virus. *Prog Brain Res* 51:51–57.
8. Dempsher J, Riker WK (1957) The role of acetylcholine in virus-infected sympathetic ganglia. *J Physiol* 139(1):145–156.
9. Kiraly M, Dolivo M (1982) Alteration of the electrophysiological activity in sympathetic ganglia infected with a neurotropic virus. I. Presynaptic origin of the spontaneous bioelectric activity. *Brain Res* 240(1):43–54.
10. McCarthy KM, Tank DW, Enquist LW (2009) Pseudorabies virus infection alters neuronal activity and connectivity in vitro. *PLoS Pathog* 5(10):e1000640.
11. Kramer T, Enquist LW (2012) Alphaherpesvirus infection disrupts mitochondrial transport in neurons. *Cell Host Microbe* 11(5):504–514.
12. Mayer ML, James MH, Russell RJ, Kelly JS, Pasternak CA (1986) Changes in excitability induced by herpes simplex viruses in rat dorsal root ganglion neurons. *J Neurosci* 6(2): 391–402.
13. Mayer ML, et al. (1985) Spontaneous electrical activity induced by herpes virus infection in rat sensory neuron cultures. *Brain Res* 341(2):360–364.
14. Granstedt AE, Szpara ML, Kuhn B, Wang SS, Enquist LW (2009) Fluorescence-based monitoring of in vivo neural activity using a circuit-tracing pseudorabies virus. *PLoS ONE* 4(9):e6923.
15. Tian L, et al. (2009) Imaging neural activity in worms, flies and mice with improved GCaMP calcium indicators. *Nat Methods* 6(12):875–881.
16. Hires SA, Tian L, Looger LL (2008) Reporting neural activity with genetically encoded calcium indicators. *Brain Cell Biol* 36(1–4):69–86.
17. Smith BN, et al. (2000) Pseudorabies virus expressing enhanced green fluorescent protein: A tool for in vitro electrophysiological analysis of transsynaptically labeled neurons in identified central nervous system circuits. *Proc Natl Acad Sci USA* 97(16): 9264–9269.
18. Banfield BW, Kaufman JD, Randall JA, Pickard GE (2003) Development of pseudorabies virus strains expressing red fluorescent proteins: new tools for multisynaptic labeling applications. *J Virol* 77(18):10106–10112.
19. Lichtman JW (1980) On the predominantly single innervation of submandibular ganglion cells in the rat. *J Physiol* 302:121–130.
20. Szpara ML, et al. (2011) A wide extent of inter-strain diversity in virulent and vaccine strains of alphaherpesviruses. *PLoS Pathog* 7(10):e1002282.
21. Pomeranz LE, Reynolds AE, Hengartner CJ (2005) Molecular biology of pseudorabies virus: Impact on neurovirology and veterinary medicine. *Microbiol Mol Biol Rev* 69(3): 462–500.
22. Ekstrand MI, Enquist LW, Pomeranz LE (2008) The alpha-herpesviruses: Molecular pathfinders in nervous system circuits. *Trends Mol Med* 14(3):134–140.
23. Curanovic D, Enquist LW (2009) Virion-incorporated glycoprotein B mediates transneuronal spread of pseudorabies virus. *J Virol* 83(16):7796–7804.
24. Tomishima MJ, Enquist LW (2001) A conserved alpha-herpesvirus protein necessary for axonal localization of viral membrane proteins. *J Cell Biol* 154(4):741–752.
25. Brideau AD, Card JP, Enquist LW (2000) Role of pseudorabies virus Us9, a type II membrane protein, in infection of tissue culture cells and the rat nervous system. *J Virol* 74(2):834–845.
26. Lyman MG, Feierbach B, Curanovic D, Bisher M, Enquist LW (2007) Pseudorabies virus Us9 directs axonal sorting of viral capsids. *J Virol* 81(20):11363–11371.
27. Lyman MG, Kemp CD, Taylor MP, Enquist LW (2009) Comparison of the pseudorabies virus Us9 protein with homologs from other veterinary and human alphaherpesviruses. *J Virol* 83(14):6978–6986.
28. Ch'ng TH, Spear PG, Struyf F, Enquist LW (2007) Glycoprotein D-independent spread of pseudorabies virus infection in cultured peripheral nervous system neurons in a compartmented system. *J Virol* 81(19):10742–10757.
29. De Regge N, et al. (2006) Alpha-herpesvirus glycoprotein D interaction with sensory neurons triggers formation of varicosities that serve as virus exit sites. *J Cell Biol* 174(2):267–275.
30. Schmitz D, et al. (2001) Axo-axonal coupling. A novel mechanism for ultrafast neuronal communication. *Neuron* 31(5):831–840.
31. Maex R, De Schutter E (2007) Mechanism of spontaneous and self-sustained oscillations in networks connected through axo-axonal gap junctions. *Eur J Neurosci* 25(11):3347–3358.
32. Ehinger B, Falck B, Sporrong B (1970) Possible axo-axonal synapses between peripheral adrenergic and cholinergic nerve terminals. *Z Zellforsch Mikrosk Anat* 107(4):508–521.

33. Smith PG, Warn JD, Steinle JJ, Krizsan-Agbas D, Hasan W (2002) Modulation of parasympathetic neuron phenotype and function by sympathetic innervation. *Auton Neurosci* 96(1):33–42.
34. Hanani M (2010) Satellite glial cells in sympathetic and parasympathetic ganglia: In search of function. *Brain Res Brain Res Rev* 64(2):304–327.
35. Campana WM (2007) Schwann cells: Activated peripheral glia and their role in neuropathic pain. *Brain Behav Immun* 21(5):522–527.
36. Chibuzo GA, Cummings JF (1980) Motor and sensory centers for the innervation of mandibular and sublingual salivary glands: A horseradish peroxidase study in the dog. *Brain Res* 189(2):301–313.
37. Granstedt AE, Brunton BW, Enquist LW (2013) Imaging the transport dynamics of single alphaherpesvirus particles in intact peripheral nervous system explants from infected mice. *mBio* 4(3):e00358–00313.
38. Smith G (2012) Herpesvirus transport to the nervous system and back again. *Annu Rev Microbiol* 66:153–176.
39. Weeks BS, Ramchandran RS, Hopkins JJ, Friedman HM (2000) Herpes simplex virus type-1 and -2 pathogenesis is restricted by the epidermal basement membrane. *Arch Virol* 145(2):385–396.
40. Reichelt M, Zerboni L, Arvin AM (2008) Mechanisms of varicella-zoster virus neuropathogenesis in human dorsal root ganglia. *J Virol* 82(8):3971–3983.
41. Szpara ML, Tafuri YR, Enquist LW (2011) Preparation of viral DNA from nucleocapsids. *J Vis Exp* (54):3151.
42. Ch'ng TH, Enquist LW (2005) Efficient axonal localization of alphaherpesvirus structural proteins in cultured sympathetic neurons requires viral glycoprotein E. *J Virol* 79(14): 8835–8846.
43. Favoreel HW, Van Minnebruggen G, Nauwynck HJ, Enquist LW, Pensaert MB (2002) A tyrosine-based motif in the cytoplasmic tail of pseudorabies virus glycoprotein B is important for both antibody-induced internalization of viral glycoproteins and efficient cell-to-cell spread. *J Virol* 76(13):6845–6851.
44. Taylor MP, Kramer T, Lyman MG, Kratchmarov R, Enquist LW (2012) Visualization of an alphaherpesvirus membrane protein that is essential for anterograde axonal spread of infection in neurons. *mBio* 3(2).
45. Hampl H, Ben-Porat T, Ehrlicher L, Habermehl KO, Kaplan AS (1984) Characterization of the envelope proteins of pseudorabies virus. *J Virol* 52(2):583–590.
46. Brideau AD, Banfield BW, Enquist LW (1998) The Us9 gene product of pseudorabies virus, an alphaherpesvirus, is a phosphorylated, tail-anchored type II membrane protein. *J Virol* 72(6):4560–4570.
47. Tirabassi RS, Enquist LW (2000) Role of the pseudorabies virus gI cytoplasmic domain in neuroinvasion, virulence, and posttranslational N-linked glycosylation. *J Virol* 74(8): 3505–3516.
48. Whealy ME, et al. (1993) Specific pseudorabies virus infection of the rat visual system requires both gI and gp63 glycoproteins. *J Virol* 67(7):3786–3797.
49. Granstedt AE, Kuhn B, Wang SS, Enquist LW (2010) Calcium imaging of neuronal circuits in vivo using a circuit-tracing pseudorabies virus. *Cold Spring Harb Protoc* 2010(4):5410.
50. Denk W, Strickler JH, Webb WW (1990) Two-photon laser scanning fluorescence microscopy. *Science* 248(4951):73–76.
51. Pologruto TA, Sabatini BL, Svoboda K (2003) ScanImage: Flexible software for operating laser scanning microscopes. *Biomed Eng Online* 2:13.